Capillarity

Vol. 1, No. 1, p. 1-10, 2018

Original article

Main controlling factors of fracturing fluid imbibition in shale fracture network

Liu Yang[1]*, Shuo Wang[1], Jianchao Cai[2], Yixiang Gan[3], Amgad Salama[4]

[1]*State Key Laboratory for Geomechanics and Deep Underground Engineering, China University of Mining and Technology (Beijing), Beijing 100083, P. R. China*

[2]*Institute of Geophysics and Geomatics, China University of Geosciences, Wuhan 430074, P. R. China*

[3]*School of Civil Engineering, The Unversity of Sydney, Sydney, NSW 2006, Australia*

[4]*Process System Engineering, University of Regina, Regina, SK, Canada*

Keywords:
Flowback efficiency
water imbibition
shale gas
fracture network
fracturing fluid

Cited as:
Yang, L., Wang, S., Cai, J., Gan, Y., Salama, A. Main controlling factors of fracturing fluid imbibition in shale fracture network. *Capillarity*, 2018, 1(1): 1-10, doi: 10.26804/capi.2018.01.01.

Abstract:
After fracturing operations, a large amount of fracturing fluid is retained in shale fracture network, resulting in low flowback efficiency. This has been attributed to the imbibition of fracturing fluid into matrix pores. However, it is unclear how the imbibition mechanism is involved, what are its governing laws and controling parameters in fracture networks? Based on the three-dimensional water imbibition theory of matrix blocks, a fracture network model is established, and a number of dimensionless controling parameters are proposed and analyzed for flowback efficiency. The results show that the imbibition characteristics of fracturing fluid in fracture network are mainly determined by two dimensionless numbers; namely, dimensionless imbibition time, fracture width, and imbibition capacity. The dimensionless imbibition time characterizes the contact time between the fracturing fluid and shale formation, which negatively correlates to the flowback efficiency. The dimensionless fracture width is the ratio of the fracture width to the rock length, which is inversely proportional to the flowback efficiency. Smaller value of the dimensionless fracture width corresponds to larger contact area of fracturing fluid and shale, leading to a lower flowback efficiency. The dimensionless imbibition capacity depicts the capacity of shale reservoirs to imbibe fracturing fluid, which has a negative linear correlation with flowback efficiency. In addition, dimensionless time and fracture width are related to the fracturing operations, and are enhanced by increasing the shut-in periods and proppant concentration. Therefore, the flowback efficiency can be controlled by changing fracturing operations. The predictive method of the flowback efficiency established here is of great significance for reservoir damage analysis and flowback regime optimization.

1. Introduction

Shale gas is an important unconventional oil and gas resource, which has been widely paid attention to more and more by the international research community (Ezulike et al., 2015). Shale reservoirs rely on horizontal well multistage fracturing to achieve commercial production (Akin et al., 2000). Fracturing technology can induce the activation of natural fracture and form fracture network, which can be used as a high-speed passages for shale gas production (Binazadeh et al., 2016). Field experiences have shown that a large amount of fracturing fluid is retained in fracture network, and flowback efficiency is generally less than 30% (Dehghanpour et al., 2013). This is related to the large amount of fracturing fluid entering matrix pores of fractured shale (Gao et al., 2018). Studying the characteristics and controlling factors of fracturing fluid imbibition in fracture network contributes to reservoir damage analysis, fracturing effect evaluation and flowback regime optimization.

The shale develops a large number of pores at micro- and nano-scales with clay minerals (Ghaderi et al., 2017). The combination of capillary pressure and osmotic pressure leads to strong imbibition effects, which can absorb a large amount of water into the matrix pores (Engle and Rowan, 2014). Capillary imbibition is related to surface tension, pore radius and contact angle, while osmotic imbibition is related to clay

*Corresponding author.
E-mail address: shidayangliu@cumtb.edu.cn (L. Yang); wangshuo0610@163.com (S. Wang); caijc@cug.edu.cn (J. Cai); yixiang.gan@sydney.edu.au (Y. Gan); amgad.salama@uregina.ca (A. Salama).

Received March 7, 2018; revised March 29, 2018; accepted April 3, 2018; available online April 10, 2018.

mineral content and type (Hu et al., 2012). For clay-rich shale, the osmotic imbibition capacity is significantly higher than the capillary imbibition capacity, which may even cause micro-fractures to propagate in the shale reservoir. The existence of micro-fractures has an important influence on the migration of shale gas and the rock mechanical properties (Ma et al., 1997; Habibi et al., 2015). During the spontaneous imbibition process within the shale, the water imbibed into the pores dissolves the salt crystals in the pores, resulting in a high salinity of retained fracturing fluid (Meng et al., 2016). Water imbibition and ion diffusion often occur simultaneously and interact with each other (Xu et al., 2018). Previous studies found that the water imbibition and ion diffusion rate have a positive linear correlation with the square root of time (Tao et al., 2018). Researchers have found that salt-rich reservoirs are often conducive to the enrichment of shale gas. Analysis of the salt dissolution and diffusion during water imbibition is of great significance for exploring the favorable area with much exploration potentials.

The flowback efficiency of fracturing fluid is closely related to the complexity of fracture network (Tao et al., 2017). The artificial network is mainly composed of a main fracture and a series of secondary fractures (Wang and Sheng, 2018). The proppant can be laid in the main fracture with good conductivity. On the contrary, the secondary fracture proppant is difficult to enter and the conductivity is weak (Xu et al., 2015). In general, the more secondary fractures develop, the higher the network complexity. For complex artificial networks, the fracturing fluid mainly remains in the secondary fractures, and the secondary fractures are difficult for fracturing fluid flowback due to low conductivity (Jiang et al., 2018). Meanwhile, the complex network has a higher fracture-matrix contact area. It also enhances the imbibition capacity of the fracturing fluid into the shale reservoir and further reduces flowback efficiency. Ghanbari et al. (2013) carried out the fracturing fluid imbibition experiments of shale reservoir. They established a theoretical model for predicting the water imbibition intensity of shale reservoir by using the equivalent principle of the network. Finally they concluded that high exposed area of network contributes to the imbibed volume of fracturing fluid and lower flowback efficiency. Zolfaghari et al. (2015) studied the relationship between the flowback fluid salinity and cumulative fluid output, and proposed a method for slit width distribution inversion based on ion diffusion theory. However, the model makes many assumptions and does not consider the interaction mechanism of water imbibition and ion diffusion.

The fracturing fluid flowback efficiency of shale gas well is related to the water imbibition characteristics and the fracture morphology (Lan et al., 2014). At present, reseachers have conducted in-depth studies on the water imbibition characteristics and influencing factors in shale matrix pores (Tian et al., 2015). However, there are few studies on the correlation between the flowback efficiency and the characteristics of fracture network. In addition, the dimensional analysis method has not been used to analyze the main controlling factors of flowback efficiency. In this paper, the fracture network model of water imbibition is established. The dimensionless parameters are proposed about flowback efficiency of fracturing fluid in shale gas wells. The analysis here also forms three-parameter evaluation method, suitable for flowback efficiency of shale gas well.

2. Methodology

2.1 Problem statement

Fracturing operations show that the flowback efficiency of shale gas wells is generally less than 30%, and some gas well has much lower flowback efficiency (even less than 5%) (Yang et al., 2016). The water imbibition of fracturing fluid into shale reservoirs is the main reason for low flowback efficiency (Yang et al., 2015). Due to the formation of complex fracture networks after shale gas fracturing operations, it is difficult to use traditional single-slit models to apply to shale gas reservoirs. The analog double-hole dual-medium model and the software Meyer seam-net model simplify each fracturing-controlled reservoir as a cube with fractures (Fig. 1), and lay proppant in the rock fracture (Fig. 2).

2.2 Mathematical model

2.2.1 Fracture network model

According to the principle of mass conservation, the volume of fracturing fluid V_{inj} injected into the formation is equal

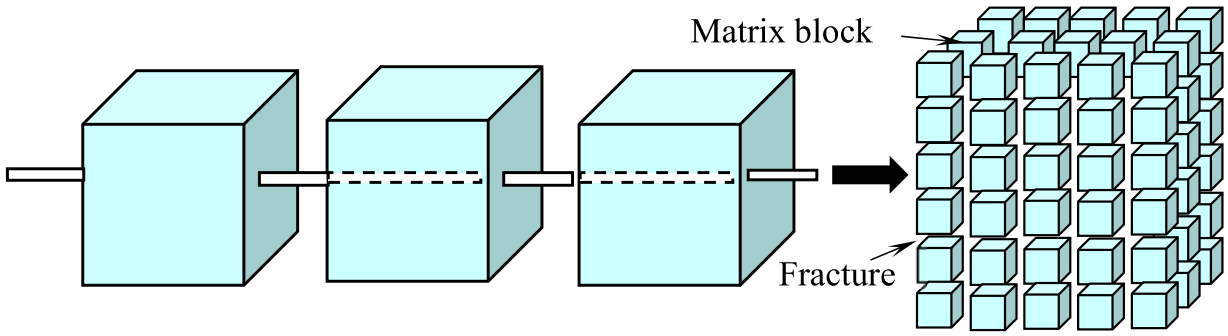

Fig. 1. Schematic diagram of volumetric fracturing model of shale gas reservoir.

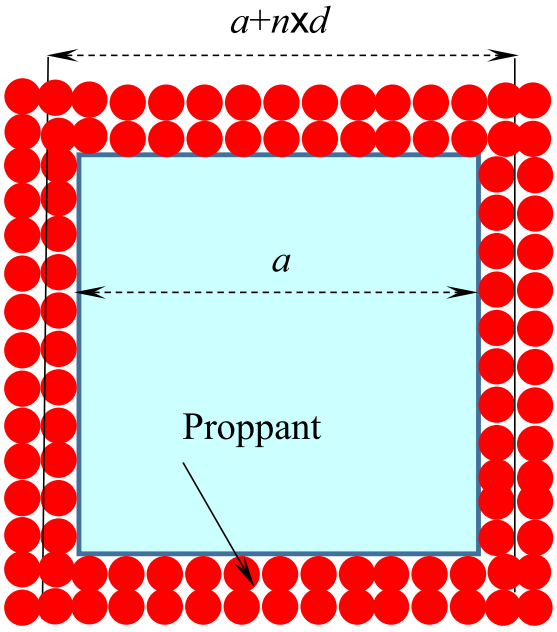

Fig. 2. Schematic diagram of the matrix block proppant laying.

to the volume of artificial fracture (due to the low permeability of the shale gas layer and the negligible fluid loss). Then the number m of rock blocks are formed by fracturing operations.

$$m = \frac{V_{inj}}{(a+nd)^3 - a^3} \tag{1}$$

where a is the length of a rock block, d and n are the diameter of a proponat particle and its number per fracture, respectively. The ratio of volume of fracturing fluid imbibed into the rock matrix block to the volume of fracturing fluid injected.

$$\begin{aligned} \frac{V_{imb}}{V_{inj}} &= \frac{m\left[a^3 - (a-2x)^3\right]\phi\left(S_{wf} - S_{wi}\right)}{m\left[(a+nd)^3 - a^3\right]} \\ &= \frac{1-(1-L_D)^3}{(1+nd/a)^3 - 1}\phi\left(S_{wf} - S_{wi}\right) \end{aligned} \tag{2}$$

where $L_D = 2x/a$ is a dimensionless length scale, S_{wf} is the final water saturation, S_{wi} is the initial water saturation, and ϕ is the porosity. Fig. 2 shows a schematic diagram of the matrix block proppant laying system. The flowback efficiency can be given by

$$1 - \frac{V_{imb}}{V_{inj}} = f\left(L_D, \frac{nd}{a}, \phi\left(S_{wf} - S_{wi}\right)\right) \tag{3}$$

It can be seen that the flowback efficiency depends on three dimensionless numbers: L_D, nd/a, and $\phi(S_{wf} - S_{wi})$. The dimensionless water imbibition time L_D is ratio of imbibition length to block side length; $nd/$a is ratio of network width to length of rock, reflecting the morphological characteristics of the fractured network; and $\phi(S_{wf} - S_{wi})$ indicates the imbibition capacity of fracturing fluid by matrix pores in shale reservoirs.

2.2.2 Matrix block imbibition model

The spontaneous water imbibition into the porous rock containing gas under capillary action and the discharge of bubbles can improve gas recovery (Handy 1960). In order to establish water imbibition model for porous rock, the following assumptions are made.

- The water imbibition process is counter-current imbibition, so the flow direction of water is opposite to the flow direction of the gas.
- Capillary-driven water imbibition can be considered as gas-water two-phase flow. Because gravity is smaller than capillary force (with relatively low Bond number), the gravity effects can be ignored.
- Capillary-driven water imbibition can be regarded as a piston displacement. The relative permeability and capillary pressure between the gas and water phases do not change with water saturation.
- The rock permeability is isotropic, regardless of the bedding effect.
- The compressibility of the gas is ignored.

According to Darcy's law, the gas and water phases flow perpendicular to the two faces in the x_1 direction, as shown in Fig. 3, are given by

$$\begin{aligned} q_g(x_1) &= 2\frac{kk_{rg}}{\mu_g}A_{x_1}\frac{dp_g}{dx_1} \\ q_w(x_1) &= 2\frac{kk_{rw}}{\mu_w}A_{x_1}\frac{dp_w}{dx_1} \\ A_{x_1} &= (a-2x)^2 \end{aligned} \tag{4}$$

where $q_g(x)$, $q_w(x)$ are the flow rates of the gas and water phases, respectively, cm^3/s; k is the absolute permeability of rock, mD; k_{rg} and k_{rw} are the relative permeability of gas and water, respectively; μ_g, μ_w are the viscosity of the gas and water, respectively, cP; P_g, P_w are the pressure of the gas and water, Pa; and A_{x1} is the cross-sectional area of the water imbibition front, cm^2. The sum of the gas phase and water phase flow rates in the x_1, x_2 and x_3 directions is given by

$$q_g = 2\frac{kk_{rg}}{\mu_g}A_{x_1}\left(\frac{dp_g}{dx_1} + \frac{dp_g}{dx_2} + \frac{dp_g}{dx_3}\right) \tag{5}$$

$$q_w = 2\frac{kk_{rw}}{\mu_w}A_{x_1}\left(\frac{dp_w}{dx_1} + \frac{dp_w}{dx_2} + \frac{dp_w}{dx_3}\right) \tag{6}$$

The gas and water phase pressure gradient between the water imbibition front and the rock block is:

$$\frac{dp_g}{dx} = \frac{dp_g}{dx_1} = \frac{dp_g}{dx_2} = \frac{dp_g}{dx_3} \tag{7}$$

$$\frac{dp_w}{dx} = \frac{dp_w}{dx_1} = \frac{dp_w}{dx_2} = \frac{dp_w}{dx_3} \tag{8}$$

The total area can be given as:

$$A_x = 6A_{x_1} \tag{9}$$

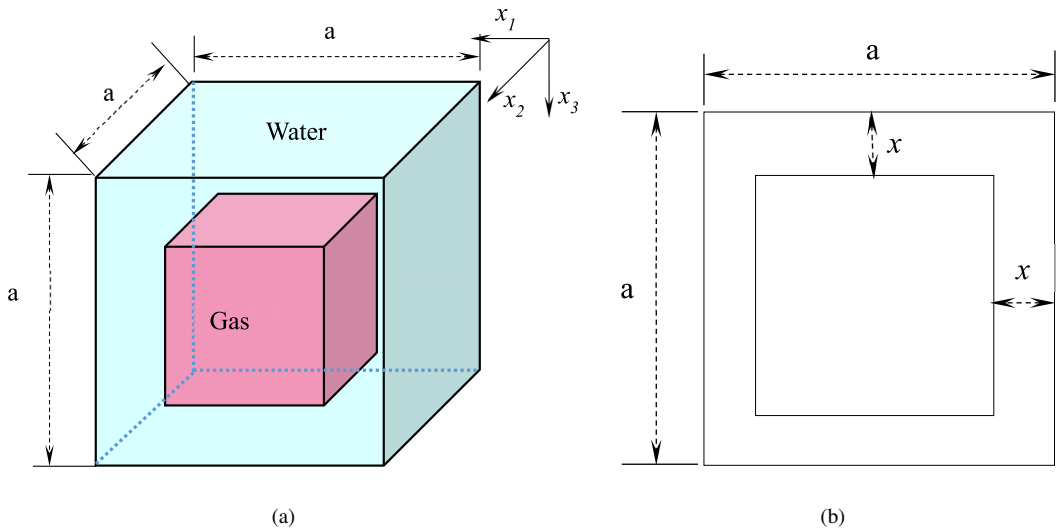

Fig. 3. Schematic diagram of counter-current imbibition of the base block.

Substituting Eqs (7), (8) and (9) into Eqs (5) and (6) yields:

$$q_g = \frac{kk_{rg}}{\mu_o} A_x \frac{dp_g}{dx} \tag{10}$$

$$q_w = \frac{kk_{rw}}{\mu_w} A_x \frac{dp_w}{dx} \tag{11}$$

For water imbibition, the volume of water imbibition is equal to the volume of gas discharge:

$$\frac{k_{rg}}{\mu_g}\frac{dp_g}{dx} = -\frac{k_{rw}}{\mu_w}\frac{dp_w}{dx} \tag{12}$$

At the gas-water interface, the relationship between gas phase and water phase pressure is:

$$p_g = p_w + p_c \tag{13}$$

where p_c is the capillary pressure at the leading edge of the water imbibition. Substituting Eq. (13) into (12), obtaining the water phase pressure gradient assuming a linear variation in capillary pressure, therefore we have:

$$q_w = kA_x \frac{1}{\frac{\mu_o}{k_{ro}} + \frac{\mu_w}{k_{rw}}} \frac{p_c}{x} \tag{14}$$

where p_c is the capillary pressure at the leading edge of the water imbibition. The water phase flow can also be characterized by the mass conservation equation (Cil and Reis, 1996). The cumulative volume of the water phase due to water imbibition is given by

$$V_{imb} = \int_0^x A_x \phi \left(S_{wf} - S_{wi}\right) dx \tag{15}$$

where S_{wf}, S_{wi} are the leading edge water saturation and initial water saturation, respectively. Deriving Eq. (15) to obtain the water flow, which is substituted into Eq. (14).

$$\frac{k}{x\phi\left(S_{wf} - S_{wi}\right)} \frac{p_c}{\left(\frac{\mu_g}{k_{rg}} + \frac{\mu_w}{k_{rw}}\right)} = \frac{dx}{dt} \tag{16}$$

Integrate Eq. (16) and the position of the water imbibition leading edge can be obtained as a function of time t:

$$x = \sqrt{\frac{2kp_c t}{\left(\frac{\mu_g}{k_{rg}} + \frac{\mu_w}{k_{rw}}\right)\phi\left(S_{wf} - S_{wi}\right)}} \tag{17}$$

Eq. (17) involves the water saturation and relative permeabilityis that is not included in the Lucas-Washburn equation. The dimensionless water imbibition length is:

$$L_D = \frac{2x}{a} = \sqrt{\frac{8kp_c t}{\left(\frac{\mu_g}{k_{rg}} + \frac{\mu_w}{k_{rw}}\right)\phi\left(S_{wf} - S_{wi}\right)a^2}} \tag{18}$$

where the capillary pressure and the characteristic pore radius are respectively expressed as:

$$p_c = \frac{2\sigma\cos\theta}{r} \tag{19}$$

$$r = \sqrt{\frac{8k}{\phi}} \tag{20}$$

where θ is contact angle and σ is surface tension. Transforming Eq. (18) and one gets:

$${L_D}^2 = t\sqrt{\frac{k}{\phi}} \frac{\sigma\cos\theta}{\left(\frac{\mu_g}{k_{rg}} + \frac{\mu_w}{k_{rw}}\right)a^2} \cdot \frac{4\sqrt{2}}{\left(S_{wf} - S_{wi}\right)} \tag{21}$$

Eq. (21) is very close to the water imbibition similarity criterion of Mattax and Kyte (1962), and it is known that Eq. (19) is expressed as:

$$L_D = \sqrt{4\sqrt{2}t_D} \tag{22}$$

Here, t_D is expressed by the following equation:

$$t_D = t\sqrt{\frac{k}{\phi}} \frac{\sigma\cos\theta}{\left(\frac{\mu_g}{k_{rg}} + \frac{\mu_w}{k_{rw}}\right)\left(S_{wf} - S_{wi}\right){L_c}^2} \tag{23}$$

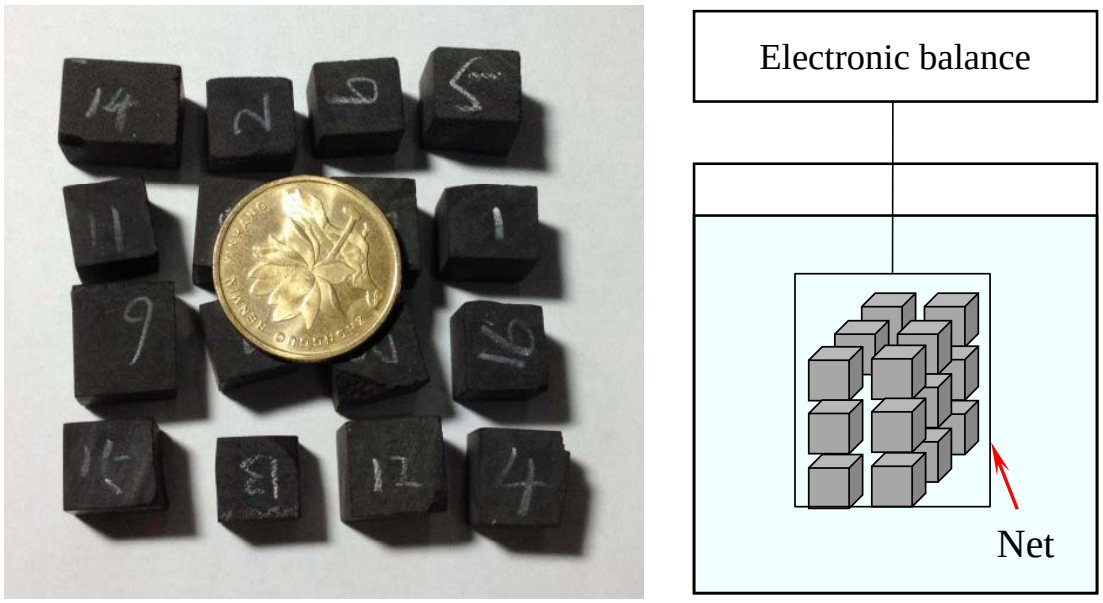

Fig. 4. Schematic diagram of cubic sample imbibition: (a) 16 samples and (b) imbibition experimens of 16 samples in one net.

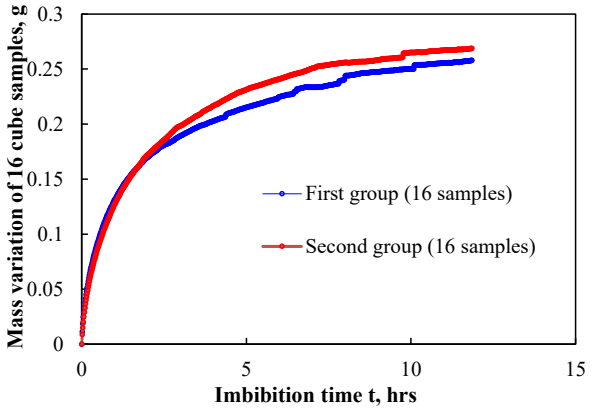

Fig. 5. Experimental imbibition results of cubic samples.

According to Mattax and Kyte (1962), the similarity criteria can directly extend the water imbibition results of sample testing in the laboratory to field. The characteristic length is L_c, which is related to the shape of experimental sample. Substitute the Eq. (23) into the Eq. (3), one gets:

$$1-\frac{V_{imb}}{V_{inj}}=1-\frac{1-\left(1-\sqrt{4\sqrt{2}t_D}\right)^3}{\left(1+nd/a\right)^3-1}\phi\left(S_{wf}-S_{wi}\right) \tag{24}$$

3. Results and discussion

3.1 Model validation

The laboratory experiments and field data were used to jointly verify the feasibility of the flowback efficiency model. The water imbibition experiment was carried out on the Lujiaping marine shale in southern China, and the samples were processed into cubes of 1 cm × 1 cm × 1 cm. In order to reduce the influence of the dimensional errors of the cube sample, in this experiment, 16 cubic samples were taken and wrapped in a net and completely immersed in water. The high-precision (0.001 g) electronic balance was used to measure the sample mass change over time. The experimental setup is shown in Fig. 4, and the results are shown in Fig. 5.

The two groups of water imbibition experiments have consistent results, indicating higher experimental repeatability. As the water imbibition time advances, the water spontaneously enters into the pores of the shale matrix, and the sample mass gradually increases. It is indicated that the water imbibition of fracturing fluid into shale reservoirs is the main reason for the generally low flowback efficiency. At the beginning of the laboratory experiment, the sample mass is increased rapidly with the soaking time. At the later stage of experiment, the sample mass did not change much and eventually tends to be stable. According to Ma et al. (1997), the laboratory experiments and the field application have the same dimensionless time:

$$[t_D]_{Lab}=[t_D]_{Field} \tag{25}$$

The samples used in the laboratory tests are taken from shale reservoirs, so the samples have the same physical properties, namely:

$$\left[\frac{t}{{L_c}^2}\right]_{Lab}=\left[\frac{t}{{L_c}^2}\right]_{Field} \tag{26}$$

The characteristic length of the base block in the formation is set to $L_{c-Field}$ = 1 m, and the characteristic length of the cubic sample in the laboratory experiment is L_{c-Lab} = 0.5 cm. The field time was t = 1 d, and the corresponding laboratory

Table 1. Basic parameters.

Permeability, mD	Porosity, %	Initial water saturation	Surface tension, (N/m)	Wetting angle, °	Fracture width, mm
1×10^{-6}	10.0	0.0	0.072	30	2
Front water saturation	Gas viscosity, mPa·s	Gas relative permeability	Water Viscosity, mPa·s	Water relative permeability	Characteristic Length, m
1.0	0.9	0.2	0.0056	0.1	1.0

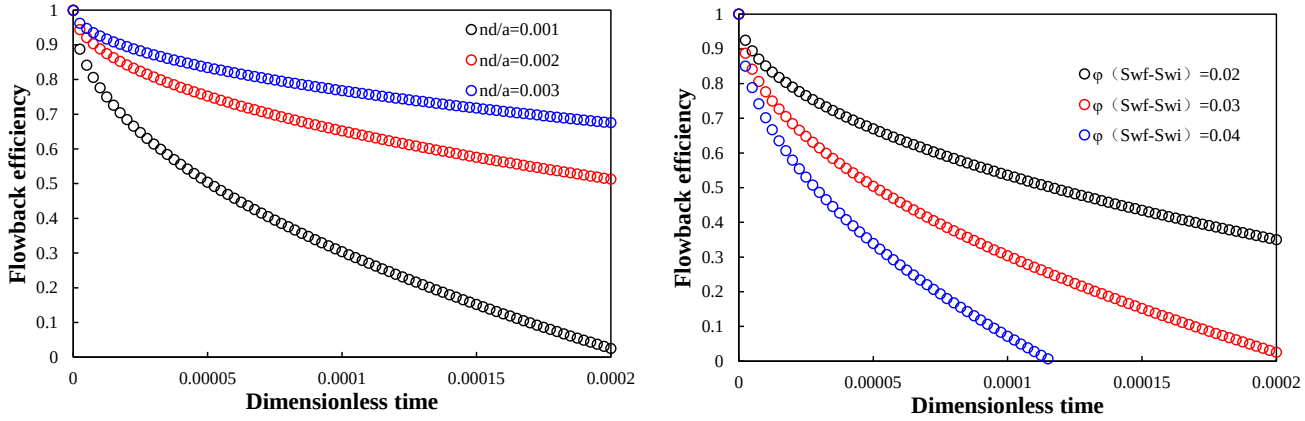

Fig. 6. Effect of dimensionless imbibition time on fracturing fluid flowback efficiency.

time was 2.16 s. According to Eq. (21) and Table 1, it can be seen that the dimensionless imbibition time t_D = 5.4 $\times 10^{-5}$ corresponds to one day in the field. The fracture width of field support is 2 mm, then nd/a = 0.002. The imbibition capacity $\phi(S_{wf} - S_{wi})$ is set to be 1.0, so the flowback efficiency is 17.5%. This is basically consistent with the conclusion that the flowback efficiency of shale gas wells in southern China is generally lower than 30%. The reason for the deviation is that the model does not consider the flow process of fracturing fluid in the fracture network. In addition, the influence of clay mineral content needs further research in future work.

3.2 Effect of dimensionless time t_D

Assume that the injected fracturing fluid volume is 10,000 m^3 and the fracturing stages are 12. The proppant is selected from 20 $\sim$ 40 mesh quartz sand. The proppant layers are calculated by taking 2 layers, 3 layers and 4 layers respectively. Since the proppants are not evenly laid, part of the proppant will be embedded in the fracture wall. So the fracture width is not exactly equal to the proppant laying height. The nd can be continuously varied to simulate the fracture width. Three reservoirs of 20-mesh quartz sand are laid with a fracture width of 3.4 mm (4 $\times$ 0.85 mm). The fracture width can be regarded as continuous variation in the range of 0 $\sim$ 3.4 mm, and the length of the rock matrix block is 1 m.

Fig. 6 shows the effect of dimensionless water imbibition time on the flowback efficiency of fracturing fluid. For a certain dimensionless fracture width and water imbibition capacity. As seen the flowback efficiency gradually decreases with the increase of the dimensionless time t_D. When the dimensionless time t_D is small, the flowback efficiency decreases rapidly, and as the t_D increases gradually, the growth rate slows down. The dimensionless time t_D primarily reflects the contact time of fracturing fluid with the shale formation. After the shale is fractured, it is often necessary to extend the shut-in periods. It can cause a large amount of fracturing fluid to imbibition into the shale formation. If the shut-in periods is long enough, the fracturing fluid will all be imbibed into the formation, and the final flowback efficiency will tend to be zero. The width of the dimensionless fracture considered in this work varies from 1×10^{-3} to 3×10^{-3}, and the flowback efficiency was rapidly enhanced. The dimensionless fracture width was positively correlated with the flowback efficiency. The water imbibition capacity was enhanced from 0.02 to 0.04, and flowback efficiency was rapidly decreased, indicating that the water imbibition capacity was negatively correlated with the flowback efficiency.

3.3 Effect of dimensionless fracture width (nd/a)

Fig. 7 shows the correlation between dimensionless fracture width and flowback efficiency. For a certain dimensionless water imbibition time t_D and water imbibition capacity, the fracturing fluid flowback efficiency gradually increases with the increase of $nd/a/$. The dimensioness width, nd/a, represents the relative width of the artificial fracture. For the same volume of fracturing fluid is injected, the larger the fracture width and the lower the artificial fracture area formed. A large amount of fracturing fluid cannot contact the formation and cannot penetrate into the formation, so the flowback efficiency

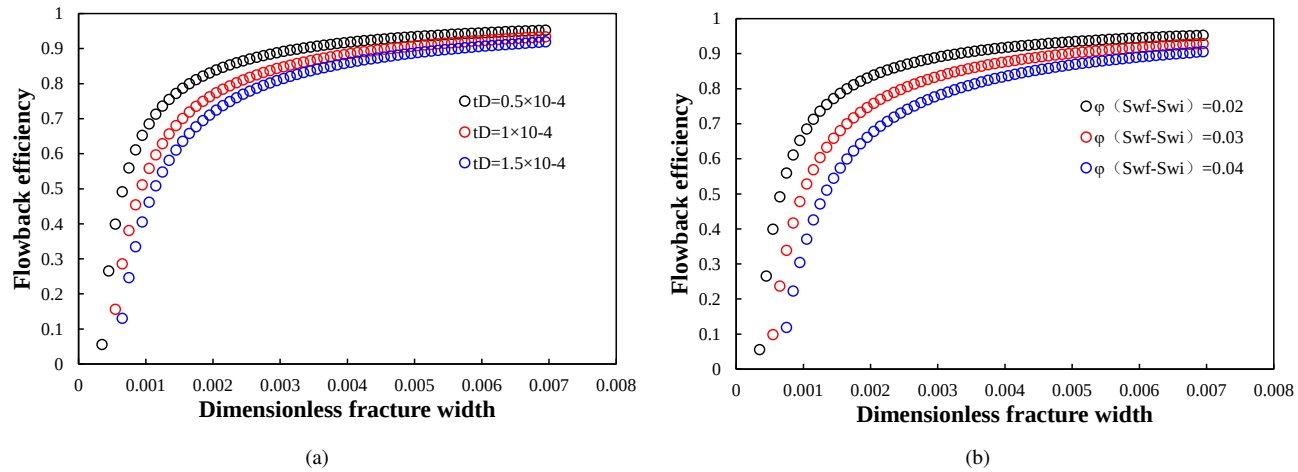

Fig. 7. Effect of dimensionless fracture width on fracturing fluid flowback efficiency.

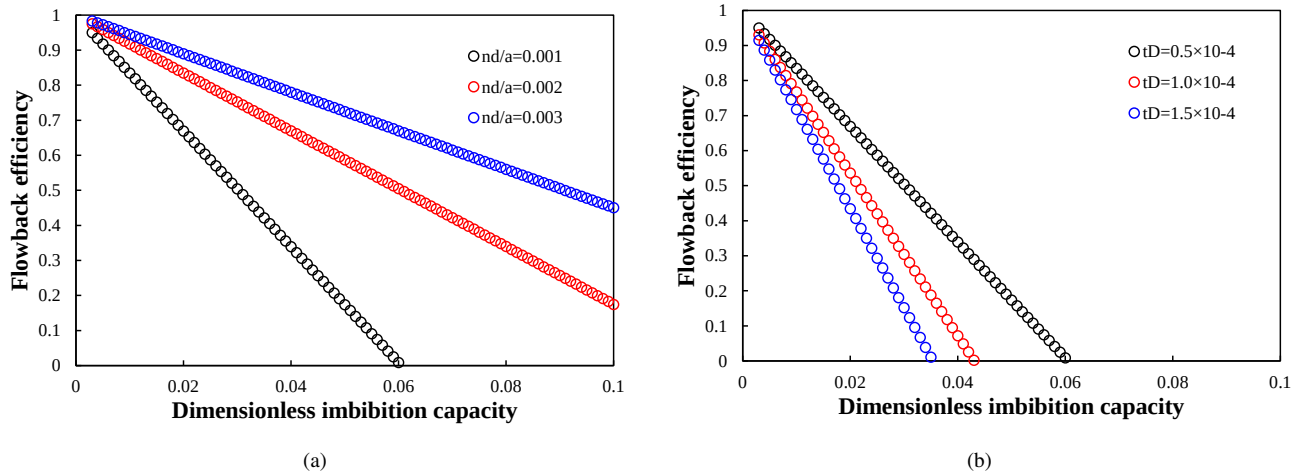

Fig. 8. Effect of dimensionless water imbibition capacity on fracturing fluid flowback efficiency.

is relatively high. When the value of nd/a is small, the flowback efficiency is enhanced rapidly. After nd/a exceeds 2, the flowback efficiency does not change substantially, and nd/a = 2 can be used as a critical value. When nd/a is less than 2, the rise of the proppant concentration is more obvious for the rise of flowback efficiency. When nd/a is greater than 2, the flowback efficiency is not significantly enhanced by increasing the proppant concentration.

3.4 Effect of dimensionless imbibition capacity

Fig. 8 shows the relationship between dimensionless water imbibition capacity $\phi(S_{wf}-S_{wi})$ and fracturing fluid flowback efficiency. Shale reservoir porosity is generally between 2% and 10%. Marine shale often has the characteristics of sub-irreducible initial water saturation, that is, the initial water saturation is lower than the irreducible water saturation, which is generally about 0 ~ 0.3. The leading edge water saturation is about 1.0. It can be seen that the water imbibition capacity range is about 0.014 to 0.1 which is suitable to the field, as shown in Fig. 8. It can be seen that the dimensionless water imbibition capacity has a linear relationship with the flowback efficiency. As the dimensionless water imbibition capacity enhances, the flowback efficiency decreases linearly. The dimensionless imbibition capacity mainly reflects the shale reservoir's capacity to accommodate the fracturing fluid. The stronger capacity corresponds to the higher proportion of imbibed fracturing fluid, resulting in the lower flowback efficiency.

For clay-rich shale, the water saturation at the leading edge is relatively high and the clay minerals have a strong water imbibition capacity. The swelling stress is generated after water imbibition, and the fracture propagation is easily induced, thereby increasing the porosity of the shale and the water saturation of the leading edge. Therefore, the presence of the clay mineral can improve the water imbibition capacity of the shale, thereby reducing the flowback efficiency of fracturing fluid. In addition, for organic-rich shale, the initial water saturation is generally low. During the shale organic generation process, a large amount of hydrocarbon gas exits the pores under high temperature and high pressure and carries

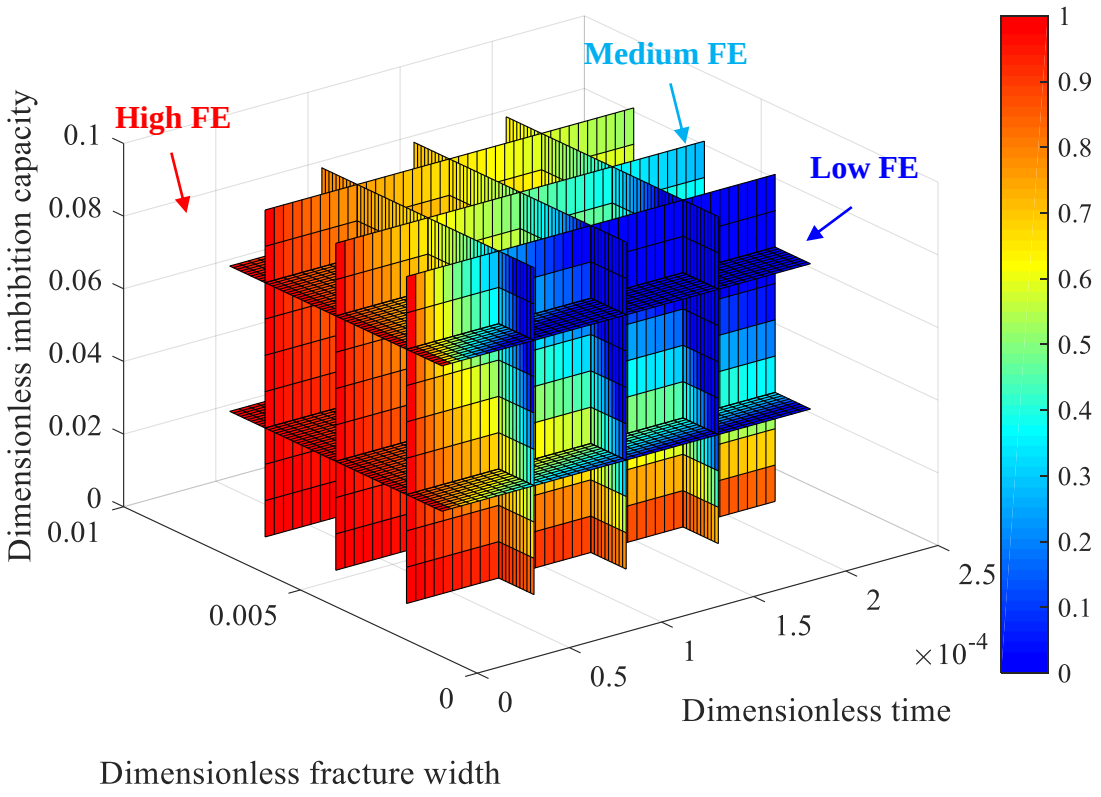

Fig. 9. Three-parameter evaluation chart of the flowback efficiency.

a large amount of water vapor. Therefore, the initial water saturation of high-quality shale reservoirs is generally low and it may be lower than the irreducible water saturation, resulting in higher water imbibition capacity of fracturing fluid.

3.5 Flowback efficiency estimation based on dimensionless parameters

A four-dimensional map generated based on the flowback efficiency model (Fig. 9). The dimensionless time t_D, the relative fracture width nd/a, and the dimensionless water imbibition capacity $\phi(S_{wf}-S_{wi})$ are respectively used as the three-dimensional coordinate axes. The graphic color reflects the flowback efficiency. Red represents a flowback efficiency of 100%, blue represents a flowback efficiency of 0, and a red to blue gradient represents a flowback efficiency of 0 to 100%. In Fig. 9, the distribution of the flowback efficiency under the influence of three parameters can be clearly shown. The red area is the high flowback efficiency area, and the blue area is the low flowback efficiency area. The shale gas wells can be classified according to the flowback efficiency (FE): high flowback efficiency (FE $>$ 0.7), medium flowback efficiency (FE $\in$ [0.4, 0.7]), and low flowback efficiency well (FE $<$ 0.4). It can be seen from Fig. 9 that the region of FE $>$ 0.7 is mainly concentrated in the region where the dimensionless time t_D is less than 5×10^{-3}. Fracture width nd/a and the imbibition capacity have little effect on the flowback efficiency. The contact time of shale with the fracturing fluid is the key to increasing flowback efficiency. The region of FE $<$ 0.4 is mainly concentrated on , imbibition capacity $>$ 0.03 and fracture width $nd/a < 5\times10^{-3}$. They are affected simutanously by three dimensionless parameters.

Field data have shown that the lower flowback efficiency of some shale gas wells results in the lower the output of shale gas. However, the lower flowback efficiency corresponds to higher production for some wells. Therefore, it is necessary to establish a reasonable flowback regime for different shale gas reservoirs. Only in this way can we control the flowback efficiency and ensure the efficient production of shale gas. It is worth noting that the dimensionless water imbibition capacity $\phi(S_{wf}-S_{wi})$ is an intrinsic parameter of the shale reservoir itself and cannot be changed by the fracturing operations. However, the change of fracturing operations can change the fracture width nd/a and dimensionless time t_D. In terms of the fracture width, nd reflects the fracture width supported by the proppant. Incresasing the amount of injected proppant enhances the fracture width and flowback efficiency. In the case of dimensionless time t_D, it reflects shut-in periods. Increasing the shut-in periods will enhance the contact time between the fracturing fluid and shale formation. So it enhances the proportion of the imbibed fracturing fluid and reduces the flowback efficiency.

4. Conclusions

In this paper, three-dimensional water imbibition model is

established based on the shale gas well fracture network, and three dimensionless parameters for controlling the fracturing fluid flowback efficiency are proposed. The main results are summarized as follows:

(1) Through dimensional analysis, it is found that the water imbibition characteristics of fracturing fluid in the fracture network mainly depend on three dimensionless numbers: dimensionless imbibition time, dimensionless fracture width, and dimensionless imbibition capacity. Dimensionless time t_D characterizes the contact time between fracturing fluid and shale. The dimensionless fracture width characterizes the ratio of the fracture width to the matrix block size length. The dimensionless imbibition capacity characterizes imbibition capacity of fracturing fluid in the shale reservoir.

(2) The dimensionless time is inversely proportional to the flowback efficiency. The dimensionless fracture width is proportional to the flowback efficiency. The dimensionless imbibition capacity has a negatively linear correlation with the flowback efficiency.

(3) The dimensionless water imbibition capacity $\phi(S_{wf} - S_{wi})$ is an intrinsic parameter of the shale reservoir itself and cannot be changed by the fracturing operations. Dimensionless time and fracture width are related to fracturing field operations. They can be controlled by changing the shut-in periods and the proppant concentration, thereby affecting the fracturing fluid flowback efficiency of the shale gas well.

Acknowledgement

The financial support of our shale research program is from the Foundation of the National Natural Science Foundation of China (No. 11702296), the Fundamental Research Funds for the Central Universities, the Major National Science, and Technology Projects of China (No. 2017ZX05049003-005).

Conflict of interest

The authors declare no competing interest.

References

Akin, S., Schembre, J.M., Bhat, S.K., et al. Spontaneous imbibition characteristics of diatomite. J. Petrol. Sci. Eng. 2000, 25(3-4): 149-165.

Binazadeh, M., Xu, M., Zolfaghari, A., et al. Effect of electrostatic interactions on water uptake of gas shales: the interplay of solution ionic strength and electrostatic double layer. Energ. Fuel. 2016, 30(2): 992-1001.

Cil, M., Reis, J.C. A multi-dimensional, analytical model for counter-current water imbibition into gas-saturated matrix blocks. J. Petrol. Sci. Eng. 1996, 16(1-3): 61-69.

Dehghanpour, H., Lan, Q., Saeed, Y., et al. Spontaneous imbibition of brine and oil in gas shales: effect of water adsorption and resulting micro fractures. Energ. Fuel. 2013, 27(6): 3039-3049.

Engle, M.A., Rowan, E.L. Geochemical evolution of produced water from hydraulic fracturing of the marcellus shale, northern appalachian basin: a multivariate compositional data analysis approach. Int. J. Coal Geol. 2014, 126: 45-56.

Ezulike, O.D., Ghanbari, E., Siddiqui, S., et al. Pseudo-steady state analysis in fractured tight oil reservoirs. J. Petrol. Sci. Eng. 2015, 129: 40-47.

Gao, L., Yang, Z., Shi, Y., et al. Experimental study on spontaneous imbibition chatacteristics of tight rocks. Adv. Geo-Energ. Res. 2018, 2(3): 292-304.

Ge, H., Yang, L., Shen, Y., et al. Experimental investigation of shale imbibition capacity and the factors influencing loss of hydraulic fracturing fluids. Petrol. Sci. 2015, 12(4): 636-650.

Ghaderi, S.M., Clarkson, C.R., Ghanizadeh, A., et al. Improved oil recovery in tight oil formations: results of water injection operations and gas injection sensitivities in the Bakken formation of southeast Saskatchewan. Paper SPE 185030 Presented at SPE Unconventional Resources Conference, 15-16 February, 2017.

Ghanbari, E., Abbasi, M.A., Dehghanpour, H. Flowback voulumetric and chemical analysis for evaluating load recovery and its impact on Early-Time Production. Paper SPE 167165 Presented at SPE Unconventional Resources Conference Cananda, Galgary, Alberta, Canada, 5-7 November, 2013.

Habibi, A., Xu, M., Dehghanpour, H., et al. Understanding Rock-Fluid interactions in the montney tight oil play. Paper SPE 175924 Presented at SPE/CSUR Unconventional Resources Conference. Calgary, Alberta, Canada, 20-22 October, 2015.

Handy, L.L. Determination of effective capillary pressure for porous media from imbibition data. Petrol. Trans. AIME 1960, 219: 75-80.

Hu, Q., Ewing, P.R., Dultz, S. Low pore connectivity in natural rock. J. Contam. Hydrol. 2012, 133: 76-83.

Jiang, Y., Shi, Y., Xu, G., et al. Experimental study on spontaneous imbibition under confining pressure in tight sandstone cores based on Low-Field nuclear magnetic resonance measurements. Energ. Fuel. 2018, 4: 56-78.

Lan, Q., Ghanbari, E., Dehghanpour, H., et al. Water loss versus soaking time: spontaneous imbibition in tight rocks. Energy Technol. 2014, 2: 1033-1039.

Ma, S., Morrow, N.R., Zhang, X. Generalized scaling of spontaneous imbibition data for strongly water-wet systems. J. Petrol. Sci. Eng. 1997, 18(3-4): 165-178.

Mattax, C.C. and Kyte, J.R. Imbibition oil recovery from fractured, water-drive reservoir. SPE J. 1962, 2(2): 177-184.

Meng, M., Ge, H., Ji, W., et al. Research on the auto removal mechanism of shale aqueous phase trapping using low field nuclear magnetic resonance technique. J. Petrol. Sci. Eng. 2016, 137: 63-73.

Tao, Z.G., Zhao, F., Wang, H.J., et al. Innovative constant resistance large deformation bolt for rock support in high stressed rock mass. Arab. J. Geosci. 2017, 10(15): 341-352.

Tao, Z.G., Zhu, C., Wang, Y., et al. Research on stability of an Open-Pit mine dump with fiber optic monitoring. Geofluids 2018, 2018: 9631706.

Tian, X., Cheng, L., Cao, R., et al. A new approach to calculate permeability stress sensitivity in tight sandstone oil reservoirs considering micro-pore-throat structure. J. Pet. Sci. Eng. 2015, 133: 576-588.

Wang, X., Sheng, J.J. A self-similar analytical solution of spontaneous and forced imbibition in porous media. Adv. Geo-Energ. Res. 2018, 2(3): 260-268.

Xu, C., Li, P., Lu, Z., et al. Discrete fracture modeling of shale gas flow considering rock deformation. J. Nat. Gas Sci. Eng. 2018, 52: 507-514.

Xu, H., Tang, D., Zhao, J., et al. A precise measurement method for shale porosity with low-field nuclear magnetic resonance: A case study of the carboniferous-Permian strata in the Linxing area, eastern Ordos Basin, China. Fuel 2015, 143: 47-54.

Yang, L., Ge, H., Shen, Y., et al. Imbibition inducing tensile fractures and its influence on in-situ stress analyses: A case study of shale gas drilling. J. Nat. Gas Sci. Eng. 2015, 26: 927-939.

Yang, L., Ge, H., Shi, X., et al. The effect of microstructure and rock mineralogy on water imbibition characteristics in tight reservoirs. J. Nat. Gas Sci. Eng. 2016, 34: 1461-1471.

Zolfaghari, A., Dehghanpour, H., Ghanbari, E., et al. Fracture characterization using flowback salt-concentration transient. SPE J. 2016, 21(1): 233-244.